Equivalent Moving Dipole Localization of Cardiac Ectopic Activity in a Swine Model during Pacing

Dakun Lai[1], **Chenguang Liu [Member, IEEE]**[1], **Michael D. Eggen**[2], **Paul. A. Iaizzo**[2], and **Bin He [Fellow, IEEE]**[1],[*]

[1] Department of Biomedical Engineering, University of Minnesota, Minneapolis, USA

[2] Department of Surgery, University of Minnesota, Minneapolis, USA

Abstract

Localization of the initial site of cardiac ectopic activity has direct clinical benefits for treating focal cardiac arrhythmias. The aim of the present study is to experimentally evaluate the performance of the equivalent moving dipole technique on non-invasively localizing the origin of the cardiac ectopic activity from body surface potential maps (BSPMs) in a well-controlled experimental setting. The cardiac ectopic activities were induced in 4 well-controlled intact pigs by either single-site pacing or dual-site pacing within the ventricles. In each pacing study, the initiation sites (ISs) of cardiac ectopic activity were localized by estimating the locations of a single moving dipole (SMD) or two moving dipoles (TMDs) from the measured BSPMs, and compared with the precise pacing sites (PSs). For the single-site pacing, the averaged SMD localization error was 18.6 ± 3.8 mm over 16 sites, while the averaged distance between the TMD locations and the two corresponding pacing sites was slightly larger (24.9 ± 6.2 mm over 5 pairs of sites), both occurring at the onset of the QRS complex (10–25 ms following the pacing spike). The obtained SMD trajectories originated near the stimulus site and then traversed across the heart during the ventricular depolarization. The present experimental results show that the initial location of the moving dipole can provide the approximate site of origin of a cardiac ectopic activity in vivo, and that the migration of the dipole can portray the passage of an ectopic beat across the heart.

Index Terms

Body surface potential mapping; electrocardiographic inverse problem; equivalent moving dipole; cardiac pacing; non-invasive localization

I. Introduction

Body surface potential mapping has been utilized to map the electrical activity of the heart for decades. Various inverse solutions have been attempted to localize and image cardiac electrical activity from the body surface potential maps (BSPMs) [1]–[7], [33]–[34]. Among them, the single moving dipole (SMD) or two moving dipole (TMD) techniques have been used to estimate and localize the focal cardiac arrhythmias with one or two well-localized sources [8]–[13], [32]–[34]. Potential clinical applications of the equivalent moving dipole technique include localization of pre-excitation sites in patients with Wolff-Parkinson-White (WPW) syndrome [14], localization of sites of myocardial infarction and foci of malignant ventricular tachycardia [15], and guiding catheter ablation [12].

[*]Correspondence: Bin He, PhD, Department of Biomedical Engineering, University of Minnesota, 7-105 NHH, 312 Church Street, Minneapolis, MN 55455, USA, Fax: 612-626-6583; binhe@umn.edu.

The moving dipole technique has been studied by many groups in simulations [11], [13], [16], [17], [31], [34], in animal preparations [18]–[20], and in human studies [14], [15], [21] since a mathematical method for fitting a dipole was first introduced by Gabor and Nelson [22]. Although promising results have been reported in experimental validation studies, limitations existed in the experimental protocols. For instance, 2-dimensional (2D) X-rays or electronic pantographs have been used to localize the surface electrodes instead of direct 3-dimensional (3D) localization [20]; the number of employed surface electrodes and the resolution of reconstructed numerical models were limited in some studies [14,20,21]; and the spherically artificial thorax model using a static simplified torso was used in some studies [18,19], which is a rough approximation of realistic geometries of individual subjects. As such, a rigorous experimental evaluation on the equivalent moving dipole technique with a well-controlled protocol is needed.

The present study represents an attempt to further evaluate the equivalent moving dipole technique by using an *in vivo* and intact large mammalian animal model (swine), whose cardiac size, heart-torso geometry, and electrophysiological characteristics were chosen to best approximate those of an adult human. A pacing protocol was used to induce well-controlled ectopic cardiac activity where the equivalent dipole solutions can be quantitatively evaluated in terms of pacing. Compared to the prior *in vitro* or *in vivo* experiments that used the isolated heart [18], [19], [30] or a relatively small animal [18], [19], the present study provides a more rigorous evaluation of the performance of the moving dipole localization in an experimental setting similar to clinical applications.

II. Methods

A. Overview of Evaluation Study

The schematic diagram of our experimental evaluation studies is shown in Fig. 1. An outline of the procedure is given below. Additional details are presented in the next sections. Experiments were carried out on four control pigs and the cardiac ectopic activities were induced in each pig by either single-site pacing or dual-site pacing within the ventricles. For each animal, both the geometrical measurements using magnetic resonance (MR) imaging and the electrical measurements using body surface potential mapping (BSPM) technique were performed so as to obtain the anatomical information and electrocardiographic (ECG) signals (see Fig. 1(a)–(c)). Afterwards, off-line data processing was performed on the recorded surface ECGs and thus the corresponding body surface isopotential maps were obtained. The boundary of the torso was constructed individually based on the acquired MRI slices (see Fig. 1(d)–(e)). Applying the cardiac equivalent source models in terms of the SMD or TMD, the body surface potentials at the surface electrode sites were forwardly calculated for each pacing site, then one or two equivalent moving dipoles were determined when the correspondingly calculated body surface potentials are the closest to the measured ones. Consequently, the initiation site (IS) at the onset of the QRS complex and the subsequent propagation of each ectopic activity were non-invasively determined by estimating the locations of the equivalent moving dipole from the measured BSPM data (see Fig. 1(f)–(g)). To investigate the performance of the equivalent moving dipole technique on localizing the origin of the cardiac ectopic activity, these estimated locations of the IS were compared with the corresponding precise pacing sites (PSs), which were recorded either with a clinical noncontact mapping system(NCM) for the pacing sites in the left ventricular (LV) or by locating the distal end of the pacing leads in the postoperative MR images of the isolated hearts for the sites in the right ventricular (RV) (see Fig. 1(h)–(k)). The 3D distances between the recorded pacing sites and the estimated dipole locations over the selected 6 beats for each pacing study were statistically analyzed.

B. Experimental Measurements

Experiments were carried out on four control pigs according to a protocol approved by the Institutional Animal Care and Use Committee (IACUC) of the University of Minnesota. The surgical preparation of these animals for hemodynamic and electrical monitoring has been previously reported [23]. During the pacing studies, each animal was anesthetized with fentanyl infused at 0.75 mcg/kg/min; all were intubated and mechanically ventilated with 65% air and 35% O_2 to maintain a $PaCO_2$ of 40 ± 2 mmHg.

Active-fixation pacing leads were implanted in both the right ventricular (RV) apex (RVA) and the RV septum (RVS) (Model 3830, Medtronic Inc., Minneapolis, MN, USA) for intramural pacing. Endocardial surface pacing from either the left ventricular apex (LVA), LV lateral wall (LVL), or LV anterior (LVAn) sites was accomplished by a quadripolar EP catheter (MarinR, Medtronic Inc.). Using two pacing leads either both inside the RV or one inside the RV and the other one inside the LV, simultaneous dual-site pacing was performed with the following pairs: RVA-RVS, RVA-LVL, RVS-LVA and RVS-LVA. The 3D locations of the LV pacing sites were recorded on the reconstructed LV geometry acquired with the noncontact mapping system(see Fig. 1(i)).

For each animal, the preoperative magnetic resonance (MR) imaging (MRI; ECG gated to end diastole) was acquired approximately 5–7 days before the *in vivo* pacing experiment so as to obtain the needed anatomical geometry information(see Fig. 1(b)). On the pacing study day, body surface potential mapping and intracavitary noncontact mapping (by the Ensite® 3000 system, St. Jude Medical Inc., St. Paul, MN, USA) were simultaneously performed during the various pacing protocols [28]. For the body surface potential mapping (see Fig. 1(c) and (e)), up to 90 disposable electrodes were placed on the anterolateral chest (see Fig. 1(a)). The body surface electrodes were referenced to the Wilson central terminal. The 3D locations of the body surface electrodes and the fiducial points were digitized directly using an electromagnetic localizer (Fastrak, Polhemus Inc., Colchester, VT, USA). After the completion of the data collection, each heart was removed and fixed in formalin in the shape of end of diastole with the intramural pacing leads remaining in place (see Fig. 1(h)). The post-operative MRI scanning was then performed on the isolated heart at least one day after the heart was fixed. After the registration between the pre-operative heart images and the post-operative heart images (method in [23]), the tip of the pacing lead localized in the post-operative heart images was projected to the pre-operative heart images and so the RV pacing site in the excitable heart model was identified.

C. Computational Methods

The Boundary Element Model—In the present study, we employed the boundary element method (BEM) to construct the numerical volume conductor model of heart and torso and solved the corresponding forward problem, which involved the calculation of the potential distribution on the body surface generated by equivalent dipoles. For each animal, the realistic three-dimensional volume conductor model was constructed individually based on the preoperative MRI scans and prior known physiological knowledge. The MR images were segmented to obtain the detailed boundaries of the heart, the lungs, and the torso, respectively (see the torso, lungs, and heart in Fig. 1(d)). Afterwards, a triangular surface mesh representation of each individual surface was computed by applying the BEM with linear triangular surface elements. Also, isotropic conductivities of 0.2, 0.04, and 0.6 S/m for the torso, the lungs, and the heart were assumed [29], respectively.

The Forward Solutions from Equivalent Dipoles—the potential at the observation point **r** due to a current dipole **p** in an infinite homogeneous medium of conductivity σ is given by [24]

$$\Phi(\mathbf{r}) = \frac{1}{4\pi\sigma} \mathbf{p} \cdot \nabla' \left(\frac{1}{|\mathbf{r} - \mathbf{r}'|} \right)$$

(1)

For the case of the bounded torso, the potential $\Phi_k(\mathbf{r})$ at the electrode locations $\mathbf{r}$ on the body surface S can be derived by applying Green's second identity [24], [25]

$$\Phi_k(\mathbf{r}) = \frac{1}{2\pi(\sigma_k^- + \sigma_k^+)} \int_{V_H} \mathbf{J}_{eq}(\mathbf{r}') \cdot \nabla' \left(\frac{1}{|\mathbf{r} - \mathbf{r}'|} \right) dV' + \frac{1}{2\pi} \sum_{l=0}^{N_s} \int_{S_L} \frac{(\sigma_k^- - \sigma_k^+)}{(\sigma_k^- - \sigma_k^+)} \Phi_k(\mathbf{r}') d\Omega_{rr'},$$

(2)

Where $\mathbf{J}_{eq}(\mathbf{r}')$ denotes the equivalent dipole sources present in the heart myocardium V_H, the torso interfaces S_s extend from 0 to N_s (with internal and external conductivities σ_k^- and σ_k^+ respectively), and $d\Omega_{rr'}$ denotes the solid angle subtended at the electrode locations, $\mathbf{r}$, by the surface element, ds', associated with r'. With the assumption that the potential is constant over each triangle face, the surface electrode point $\mathbf{r}$ may be placed at the centroid of each triangle, and an equation such as Eq. (2) can be written as $\mathbf{r}$ is moved from triangle to triangle. Thus, The ensemble of N_T equations, where N_T is the total number of triangles, can be represented by the following matrix equation [25]:

$$\mathbf{\Phi} = \mathbf{G} + \mathbf{A}\mathbf{\Phi}$$

(3)

where $\mathbf{\Phi}$ is an $N_T \times 1$ matrix of the desired triangle potentials, $\mathbf{G}$ is an $N_T \times 1$ matrix containing the first terms on the right hand side of Eq. (2), and $\mathbf{A}$ is an $N_T \times N_T$ matrix that depends only on torso geometry and conductivities. In order to get the solution of $\mathbf{\Phi}$, the Eq. (3) can be rewritten as $(\mathbf{I} - \mathbf{A})\mathbf{\Phi} = \mathbf{G}$, where $\mathbf{I}$ is an $N_T \times N_T$ identity matrix. Since Eqation (3) is singular, the deflation technique proposed by Lynn and Timlake [26] was applied in this study. A unique forward solution of body surface potentials at the electrode locations was thus obtained from dipole source in the heart.

The Inverse Moving Dipole Computation—A dipolar current source is characterized by six parameters: its X, Y, Z coordinates and its dipolar components P_x, P_y, P_z. One or two equivalent moving dipoles, used to represent cardiac electrical activity, are defined as the one or two dipoles whose resultant body surface potentials would be the closest to the measured ones. In the present study, the calculation of parameters of the SMD or TMD was performed during the QRS complex. This solution compares the measured surface potentials $\tilde{\mathbf{\Phi}}_i$ at a surface electrode location i, to the corresponding computed surface potentials $\mathbf{\Phi}_i$ from the assumed SMD (or TMD) source. The optimal dipole is defined as the one that minimizes the following:

$$F = \sum_{i=1}^{N} ||\tilde{\mathbf{\Phi}}_i - \mathbf{\Phi}_i||^2$$

(4)

The number of measuring sites N (around 80–90) is greater than the number of parameters in the dipole model (6 for the SMD model and 12 for the TMD model). Therefore, minimizing F is equivalent to the least-squares error solution of an overdetermined set of N equation system. The parameters of the equivalent dipole(s) (the SMD or TMD) can be determined by solving Eq. (3) when F in Eq. (4) is minimum.

The Source Localization by Moving Dipole—In the moving dipole localization, the initial guess of the dipole's location was set at the geometric center of the heart. The dipole was then shifted and scaled to minimize the residual between the measured and computed body surface potentials. The shifting and scaling was guided by a nonlinear optimization method introduced by Nelder and Mead [27] as implemented by using an improved boundary element method [31] in the CURRY (Compumedics, Charlotte, NC, USA) software package in the present study, where the searching progress for the optimal site of an equivalent current dipole usually took no longer than 1 s with a Pentium 4. The computed locations of the equivalent dipoles vary from time to time, which offers an important capability to localize the regions of myocardial tissues which are most responsible for the measured BSMPs. Thus, the SMD and TMD solutions also referred to as source localizations in the electrocardiogram inverse problem literature. In the present study, off-line data processing was performed firstly on the recorded BSPM data; then, the moving dipole inverse problems were solved with the help of the CURRY software. For each pacing study, six well-captured beats were selected for analysis. Those beats were further preprocessed to remove noise and baseline shift. Next, the SMD or TMD model was used to compute the inverse solutions at every time instant of the QRS interval of each obtained single-site pacing or dual-site pacing beat, respectively. The temporal resolution of the solutions was 1 ms. In the present study, the onset instant of the QRS complex of each ectopic beat that corresponds to the initiation of activation was manually determined at the time when the magnitude of the measured surface potentials is apparently larger than that of noise. Therefore, the initiation sites (ISs) of activation could be obtained from the SMD or TMD locations calculated from the BSPM at the onset of the QRS complex. The subsequent propagation of electrical activities was depicted in terms of a dipole trajectory consisting a series of SMDs during the ventricular depolarization (see Fig. 1(g)).

D. Evaluation of the Moving Dipole Solutions

The performance of the moving dipole approach was evaluated in terms of the localization errors (LE) of the ISs of the paced ectopic activity. The LE statistical analysis included measuring the 3D distances $D_i (D_i = \sqrt{D^2_{ix} + D^2_{iy} + D^2_{iz}}$, where x, y, and z are corresponding to the axis X, Y, and Z, respectively) between the pacing sites and estimated dipole locations over the selected i ($i=1, 2, 3\ldots n$) beats for each pacing study. Then, the overall median distance D_m was estimated from the following equation:

$$D_m = \frac{1}{n}\sum_{i=1}^{n}\sqrt{D^2_{ix} + D^2_{iy} + D^2_{iz}}$$

(5)

and the overall standard deviation (SD) was obtained from:

$$S_d = \sqrt{\frac{\sum_{i=1}^{n}(D_i - D_m)^2}{n-1}}$$

(6)

Importantly, the real location of each pacing site (PS) was obtained by the following procedure.

In each pacing study, the origin of cardiac activation was localized by inversely estimating the locations of a single moving dipole or two moving dipoles in the individual heart-torso volume models, and compared with the actual sites obtained independently from the NCM system (see Fig. 1(i)) or the postoperative MR images. For the pacing stimuli in the RV, the precise locations of pacing sites were obtained by locating the distal end of the pacing leads in the postoperative

MR images of the isolated hearts (see Fig. 1(h)). Note that each heart was fixed in an end-diastolic state and the geometric model was reconstructed from the postoperative MR images. Then, an image co-registration procedure between the isolated, fixed hearts and the beating hearts was performed to determine the precise 3D locations of the pacing sites in the resultant heart-torso models. Also, each heart was paced at endocardial locations within the LV with an EP catheter. The precise locations of the endocardial pacing sites and the endocardial geometries of the LV were both recorded by the NCM system. In order to determine the precise locations of the pacing sites reflected in the resultant heart-torso models, the endocardial surface maps were extracted from the NCM recordings and then registered with the corresponding surface of the beating heart segmented from the preoperative MR images. The rigid co-registration approach used here for the LV pacing sites and the RV pacing sites was the same as that used in our previous study [23]. After the registration, the precise locations of the pacing sites within either the RV or the LV were determined in the heart-torso model and could be directly compared with the estimated locations.

Information about the activation sequence after the onset of the QRS complex was also estimated by spatially visualizing the migration of the equivalent dipoles during depolarization within the heart. Each dipole was spatially superimposed on the individual heart geometry. The moment of the dipole was scaled proportionally by the magnitude of the dipole and the activation instant was scaled by color.

III. Results

A. Experimentation and Modeling

The present study was conducted on four well-controlled pigs. The numerical heart-torso volume conductor model was constructed for each animal based on their individual pre-operative MR images. Each model consisted of the boundary surfaces of the heart, the lungs and the torso, and contained over 5,000 triangular boundary elements (Note that the heart chambers were also segmented in each model and shown in figures 1–4). A summary of the modeling and experimental parameters can be found in Table 1.

B. Endocardial LV Pacing

Endocardial pacing was successfully conducted within the LV in all four animals. Figure 2 depicts an example of the measurements, the modeling and the SMD localization results when the heart is paced from the LV lateral. In Fig. 2A, the individual heart-torso volume conductor model and the body surface ECGs are presented, including one beat under sinus rhythm (the first one) and three beats when the heart is captured by pacing (the last three). The displayed ECGs are recorded by 12 surface electrodes during experiment, which are marked on the volume conductor model from the total of 88 electrodes. The SMD inverse analysis was applied on the collected BSPM data (corresponding to the second beat in Fig. 2A), and the constructed isopotential contour maps and estimated SMD are shown in Fig. 2B (during ventricular depolarization). In the isopotential maps, the isopotential contour lines with an increment of 0.05 mV are shown partly at an interval of 20 ms during the depolarization (17 ms–76 ms, see panel (i) of Fig. 2B). The zero potential contour is identified by a black trace, and the red lines and the blue lines depict the positive and negative isopotential contour area, respectively. The innermost red or blue contours indicate the positions of the maximum or minimum. Specifically, the potential range for each potential isochrone is shown as the 'P_Range' between the minimum and maximum value of the surface potential. Moreover, the inverse solutions of the SMD are obtained for every sampling instant and shown in terms of the dipole trajectory during depolarization (17 ms–76 ms, see panel (ii) of Fig. 2B). Each dipole of this trajectory is of the corresponding result of the SMD localization at that instant, which includes the 3D location within the heart, magnitude-scaled size, and color-scaled activation instant.

The estimated initial site of the depolarization is labeled with 'IS' (the earliest dipole of the trajectory displayed in dark blue) and compared to the precise location of the pacing site indicated by a green ball labeled with 'PS'. The maximum and minimum magnitudes of the dipole obtained during the depolarization procedure are shown as 'D_min' and 'D_Max', respectively. As shown in panel (ii) of Fig. 2B, the excitation starts from the LV lateral, develops across the ventricles, and reaches the basal area of the RV the 76 ms after pacing. At the end of the QRS complex, the dipole was near the upper free wall of the RV and oriented toward the upper posterior. In panel (i) of Fig. 2B, the body surface isopotential contour maps show a movement of the projected cardiac activation away from the left-anterior surface of the torso to the right side, and then toward the posterior area at the end of the QRS complex, which is closely related to the revealed propagation by the SMD trajectory..

In total, ten endocardial sites within the LV were paced, and 60 paced beats were analyzed (6 for each site). The estimation results are summarized in Table 2. Over the 60 beats analyzed, the averaged localization error of the initial site of activation was 18.4 ± 3.4 mm at the onset of QRS (10–25 ms after the pacing spike).

C. Intramural RV Pacing

Intramural pacing in the RV was successfully completed in all four animals. Figure 3 depicts an example of the isopotential contour maps that was observed when the heart was paced at the RV apex, and the corresponding results of the SMD localization where physiologically reasonable SMD trajectories were observed during the QRS interval. In total, six intramural sites within the RV were paced, and 36 paced beats were analyzed (6 for each site). The estimation results are also summarized in Table 2. Over the 36 beats analyzed, the averaged localization error of the initial site of activation was 18.9 ± 4.6 mm at the onset of the QRS complex (11–23 ms after the pacing spike).

D. Simultaneous Dual-site Pacing

Simultaneous dual-site pacing either within a single-chamber (both sites within the RV) or dual chambers (one from the RV and the other from the LV) was successfully completed in two animals. Figure 4A displays an example of the estimated locations of the initial sites with the TMD model during simultaneous RVA-RVS pacing. The 3D distances between each of the two separate pacing sites (the green balls, marked with 'PS_RVA' and 'PS_RVS', separately) and two estimated dipoles (the red pole marked with 'IS_RVA' and the blue pole marked with 'IS_RVS') are shown for evaluating the localization errors. Another example of dual-site pacing is shown in Figure 4B, where the heart was simultaneously paced at the RV septum and the LV apex. In total, five pairs of single-chamber or dual-chamber dual sites were paced, and 30 paced beats were analyzed (6 for each pair). The evaluation results of the accuracy of the TMD localizations are summarized in Table 3. Over the 30 beats analyzed, the averaged localization error of the initial sites of the corresponding ectopic foci was 24.9 ± 6.2 mm at the onset of the QRS complex (10–25 ms after the pacing spike).

IV. Discussion

Localization of cardiac ectopic activity has direct clinical benefits for treating focal cardiac arrhythmias. It has been suggested previously that the equivalent SMD or TMD approach is only appropriate when the cardiac sources themselves consist of one or two well-located centers of activity or during their early stage, respectively [1]. With state-of-the-art technologies and a well-controlled experimental protocol using large mammalian animal, we revisited this idea in this work, in an attempt to rigorously assess the accuracy and reliability of approximating cardiac electrical activity using the equivalent moving dipole model. To our knowledge, the present study represents the first reported effort to rigorously evaluate the performance of the

moving dipole inverse technique on localizing focal cardiac activity in a pre-clinical setting. Specifically, we chose the *in vivo* swine model in this study because of its close approximation to human cardiac size, heart-torso geometry, and electrophysiological characteristics (versus those of the rabbit, turtle, or canine). And, the 3D locations of these pacing sites within the LV or RV are precisely recorded by a clinical NCM system during experiments or directly marked out by the postoperative MR images of the isolated heart, and subsequently used as a reference to quantitatively evaluate the localization accuracy of the SMD or TMD approaches. The present results suggest that: 1) the equivalent moving dipole technique is capable of localizing the source of a cardiac ectopic beat in its early stage, 2) the localization error of either the SMD or TMD technique was about 20 mm, and 3) the SMD trajectories originate near the stimulus site and then traverse across the heart during the QRS complex.

A. Localization of Initial Site

The present study represents an attempt to experimentally evaluate the performance of the moving dipole inverse technique on localizing the initial site of cardiac ectopic activity in a well-controlled setting. Such confirmations in a pre-clinical study would be expected to provide a more realistic evaluation which may have stronger clinical implications and more reliable results than previous evaluations in animal models or human patients. Previously, Using an isolated electrolyte-perfused rabbit heart in a spherical chamber preparation 63.5 mm in diameter, Ideker *et al* [8] reported a distance of 3.7 mm (range 2.6–4.6 mm) between the estimated SMD location and a subepicardial pacing site in the LV. Savard *et al* [20] assessed the accuracy of SMD evaluation for the ectopic case in an intact *in vivo* canine model and obtained an averaged distance of 19 ± 8 mm between the initial SMD vector and the stimulation electrode. Later, they conducted a series of studies on 14 patients with pacemakers and found that the averaged distance between the SMD location at the onset of the QRS complex and the pacing electrode was 31 mm, or a higher accuracy of 25 ± 8 mm if the torso model included lung inhomogeneities [21]. At the same time, very few studies were conducted on the TMD localization of cardiac ectopic activity with two separate foci. Mirvis *et al* [9] used the isolated heart in the same experimental preparation as Ideker *et al*'s studies [8], [30] to test the ability of the TMD model to localize two burns and reported that the localization errors were 4.2 ± 2.6 mm and 5.7 ± 4.9 mm from the first and second burn, respectively. Differences in study settings between the present study and other previous studies may lead to different interpretations of results. For the early studies *in vitro* isolated rabbit [8], [18] or turtle heart [19], the relative small size of the heart-torso may result in a smaller scale of localization error. For the *in vivo* intact dog experiments [20], the previous researchers used the same geometric torso from the first animal for all animals, in which the variation in torso geometry between individual animals was neglected. Furthermore, the methods used to obtain the exact locations of the surface recording and/or intracardiac stimulation electrodes, such as fluoroscopic projections or electronic pantograph, are relatively inaccurate. In the present study, a high-resolution heart-torso model was constructed for each individual animal from the preoperative MR images. Intracavitary noncontact mapping during experiments and postoperative MR imaging of each isolated heart were also performed to obtain the precise locations of the pacing sites within the LV and RV, respectively. The precise locations of the surface electrodes were determined directly using an 3D electromagnetic localizer with an high accuracy of less than 1 mm. Thus, many factors affecting the accuracy of the SMD and TMD evaluation were minimized in the experimental protocols. Meanwhile, for potential clinical applications, conditions met in this study such as an *in vivo* and intact large mammalian model, variously simulated cardiac ectopic activities, and near-clinical cardiac catheterization settings with a clinical NCM system, also provide a more valuable consideration of the efficiency of the localization performance of the moving dipole technique. It also appears that the TMD inverse solution could be useful in providing an alternative method for localizing the trajectory of dual accessory pathways in WPW patient or two separate ectopic foci. When more than one

arrhythmogenic activity (e.g., two pre-excitation site or fusion beat) are taking place simultaneously, one would need to know the locations of these electric events before surgical or catheter ablation.

B. Representation of Activation Sequence

In the present study, we additionally investigated the propagated activation wavefronts after the onset of the QRS complex by 3D visualization of a SMD trajectory (two typical examples are shown in Figure 2 and Figure 3). The dipole trajectory consists of a series of SMD solutions where the dipoles' locations, orientations and magnitudes were determined at every sampling instant during depolarization. All dipoles were displayed in the individual realistic heart geometry with the endocardial and epicardial surfaces. The revealed migrations of activation wavefronts in the present study are in good agreement with the known knowledge about cardiac electrophysiology; they are also consistent with the recorded BSPMs, which were reported in the previous investigations by Savard *et al* [20], [21], Ideker *et al* [30], and Mirvis *et al* [15].

C. Study Limitations

Although employing the NCM system within the present protocol provides benefits for testing the method of the equivalent moving dipole solutions in a setting similar to clinical study in patients, it also represents a limitation that we do not have direct measurements within the 3D ventricular volume. As described in the Methods section, in order to determine the endocardial pacing sites in the heart-torso model, the endocardial surface recorded by the NCM system was registered with the corresponding surface of the beating heart segmented from the pre-operative MR images. Although both of the endocardial surfaces correspond to the end of diastole, they cannot exactly match due to the complex positional and size changes that may occur during the cardiac and respiratory cycles. Because of this problem, errors might be introduced when the registration procedure is applied.

Due to the limited capability of the employed software CURRY on representing two successive propagated activation wavefronts, the TMD trajectories were not further investigated. Instead, two separate ectopic foci were successfully localized in the TMD study. It would be of interest to trace two moving dipoles simultaneously in future studies.,

V. Conclusion

In summary, the present study provides an insight into the clinical applicability of the moving dipole localization techniques, such as clinical pre-diagnosis of focal arrhythmias, guiding placement of endocardial mapping aiding catheter ablation, etc. The present results suggest that the single-dipole representation could portray the origin and propagation of an ectopic wavefront across the heart and that the two-dipole inverse solution could localize two ectopic foci with reasonable accuracy. The equivalent moving dipole solutions have the potential to noninvasively estimate the anatomical origin of certain types of cardiac disorders that can be well-represented by a dipolar source. Particularly relevant applications include the localization of one or two accessory pathways from the pre-excited delta wave observed in the WPW syndrome and the determination of the site of origin of ventricular tachycardia. Further investigations should be done to conduct clinical studies on patients with one or two ectopic foci and the results should be compared with other ECG inverse solutions.

Acknowledgments

References

1. Gulrajani RM, Roberge FA, Savard P. Moving dipole inverse ECG and EEG solutions. IEEE Trans Biomed Eng Dec;1984 31(12):903–910. [PubMed: 6396217]

2. Burnes JE, Taccardi B, Rudy Y. A noninvasive imaging modality for cardiac arrhythmias. Circulation 2000;102:2152–2158. [PubMed: 11044435]

3. He B, Wu D. Imaging and visualization of 3D cardiac electric activity. IEEE Trans Inf Technol Biomed Sept;2001 5(3):181–186. [PubMed: 11550839]

4. Li G, He B. Localization of the site of origin of cardiac activation by means of heart-model-based electrocardiographic imaging approach. IEEE Trans Biomed Eng Jun;2001 48(6):660–669. [PubMed: 11396596]

5. He B, Li G, Zhang X. Noninvasive three-dimensional activation time imaging of ventricular excitation by means of a heart-excitation-model. Phys Med Biol Nov;2002 47:4063–4078. [PubMed: 12476982]

6. Tilg B, Fischer G, Modre R, Hanser F, Messnarz B, Schocke M, Kremser C, Berger T, Hintringer F, Roithinger FX. Model-based imaging of cardiac electrical excitation in humans. IEEE Trans Med Imag Sept;2002 21(9):1031–1039.

7. Zhang X, Ramachandra I, Liu Z, Muneer B, Pogwizd SM, He B. Noninvasive three-dimensional electrocardiographic imaging of ventricular activation sequence. Am J Physiol Heart Circ Physiol 2005;289(6):H2724–H2732. [PubMed: 16085677]

8. Ideker RE, Bandura JP, Larsen RA, Cox JW, Keller JW, Brody DA. Localization of heart vectors produced by epicardial burns and ectopic stimuli: validation of a dipole ranging method. Circ Res 1975;36:105–112. [PubMed: 1116214]

9. Mirvis DM, Keller FW, Ideker RE, Cox JW Jr, Dowdie RF, Zettergren DG. Detection and localization of multiple epicardial electrical generators by a two-dipole ranging technique. Circ Res 1977;41:551–557. [PubMed: 902361]

10. Okamoto Y, Teramachi Y, Musha T. Limitation of the inverse problem in body surface potential mapping. IEEE Trans Biomed Eng 1983;30(11):749–754. [PubMed: 6662531]

11. Hren R, Stroink G, Horacek BM. Accuracy of single-dipole inverse solution when localizing ventricular pre-excitation sites: simulation study. Med & Biol Eng & Comput 1998;36:323–329. [PubMed: 9747572]

12. Armoundas AA, Feldman AB, Mukkamala R, Cohen RJ. A single equivalent moving dipole model: an efficient approach for localizing sites of origin of ventricular electrical activation. Ann Biomed Eng 2003;31:564–576. [PubMed: 12757200]

13. Fukuoka Y, Oostendorp TF, Sherman DA, Armoundas AA. Applicability of the single equivalent moving dipole model in an infinite homogeneous medium to identify cardiac electrical sources: a computer simulation study in a realistic anatomic geometry torso model. IEEE Trans Biomed Eng 2006;53:2436–2444. [PubMed: 17153200]

14. Gulrajani RM, Huy-Pham H, Nadeau RA, Savad P, Guise JD, Primeau RE, Roberge FA. Application of the single moving dipole inverse solution to the study of the Wolff-Parkinson-White syndrome in man. J Electrocardiol 1984;17:271–288. [PubMed: 6481281]

15. Mirvis DB, Holbrook MA. Body surface distributions of repolarization potentials after acute myocardial infarction. III. Dipole ranging in normal subjects and in patients with acute myocardial infarction. J Electrocardiol 1981;17:387–398. [PubMed: 7299309]

16. Savad P, Mailloux GE, Roberge FA, Gulrajani RM, Guardo B. A simulation study of the single moving dipole representation of cardiac electrical activity. IEEE Trans Biomed Eng 1982;29:700–707. [PubMed: 7173934]

17. Jazbinsek V, Hren R, Stroink G, Horacek BM, Trontelj Z. Value and limitations of an inverse solution for two equivalent dipoles in localizing dual accessory pathways. Med & Biol Eng & Comput 2003;41:133–140. [PubMed: 12691432]

18. Mirvis DM, Keller FW, Ideker RE, Zettergren DG, Dowdie RF. Equivalent generator properties of acute ischemic lesions in the isolated rabbit heart. Circ Res 1978;42:676–685. [PubMed: 639190]

19. Brody DA, Warr OS III, Wennemark JR, Cox JW Jr, Keller FW, Terry FH. Studies of the equivalent cardiac generator behavior of isolated turtle hearts. Circ Res 1971;29:512–524. [PubMed: 5120615]

20. Savard P, Roberge FA, Perry JP, Nadeau RA. Representation of cardiac electrical activity by a moving dipole for normal and ectopic beats in the intact dog. Circ Res 1980;46:415–425. [PubMed: 7357696]

21. Savad P, Ackaoui A, Gulrajani RM, Nadeau RA, Roberge FA, Guardo R, Dube B. Localization of cardiac ectopic activity in man by a single moving dipole: comparison of different computation techniques. J Electrocardiol 1985;18:211–222. [PubMed: 4031724]

22. Gabor D, Nelson CV. Determination of the resultant dipole of the heart from measurements on the body surface. J Appl Phys 1954;25:413–416.

23. Liu C, Skadsberg ND, Iaizzo PA, He B. Estimation of global ventricular activation sequences by noninvasive three-dimensional electrical imaging: validation studies in a swine model during pacing. J Cardiovasc Electrophysiol 2008;19:535–540. [PubMed: 18179521]

24. Gulrajani RM. The forward and inverse problem of electrocardiography. IEEE Eng Med Biol Sept; 1998 17(5):84–101.

25. He, B. Modeling and Imaging of Bioelectrical Activity: Principles and Applications. New York: Kluwer Academic/Plenum Publishers; 2004.

26. Lynn MS, Timlake WP. The use of multiple deflation in the numerical solution of singular systems of equations with application to potential theory. SIAM J Numer Anal 1968;5:303–322.

27. Nelder JA, Mead R. A simplex method for function minimization. The Computer Journal 1965;7:308–313.

28. Schilling RJ, Peters NS, Davies DW. Simultaneous endocardial mapping in the human left ventricle using a noncontact catheter: comparison of contact and reconstructed electrograms during sinus rhythm. Circulation 1998;98:887–898. [PubMed: 9738644]

29. Geddes LA, Baker LE. The specific resistance of biological material: a compendium of data for the biomedical engineer and physiologist. IEEE Trans Biomed Eng 1967;5:271–293.

30. Ideker RE, Bandura JP, Cox JW Jr, Keller FW, Mirvis DM, Brody DA. Path and significance of heart vector migration during QRS and ST-T complexes of ectopic beats in isolated perfused rabbit hearts. Circ Res 1977;41:558–564. [PubMed: 902362]

31. Fuchs M, Drenckhahn R, Wischmann H-A, Wagner M. An improved boundary element method for realistic volume-conductor modeling. IEEE Trans Biomed Eng 1998;45(8):980–97. [PubMed: 9691573]

32. Dutz S, Bellemann M, Leder U, Haueisen J. Passive vortex currents in magneto- and electrocardiography: comparison of magnetic and electric signal strengths. Phys Med Biol 2006;51:145–151. [PubMed: 16357437]

33. Xanthis CG, Bonovas PM, Kyriacou GA. Inverse Problem of ECG for Different Equivalent Cardiac Sources. PIERS Online 2007;3(8):1222–1227.

34. Armoundas AA, Feldman AB, Mukkamala R, He B, Mullen TJ, Belk PA, Lee YZ, Cohen RJ. Statistical accuracy of a moving equivalent dipole method to indentify sites of origin of cardiac electrical activation. IEEE Trans Biomed Eng 2003;50(12):1360–1370. [PubMed: 14656065]
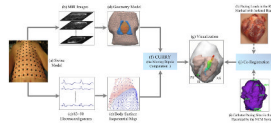
Figure 1.
Schematic diagram of electrocardiogram inverse solution and evaluation procedure (Note that the rigid co-registration approach used here for the LV pacing sites and the RV pacing sites was the same as that used in our previous study [23]). IS represents the estimated 'initiation site' of the ectopic activity, PS represents the 'pacing site' recorded by the intracavitary noncontact mapping (NCM) system, and AS represents the estimated 'activation sequence' of the ectopic activity using a dipole trajectory.
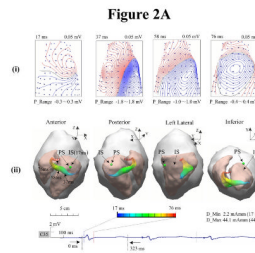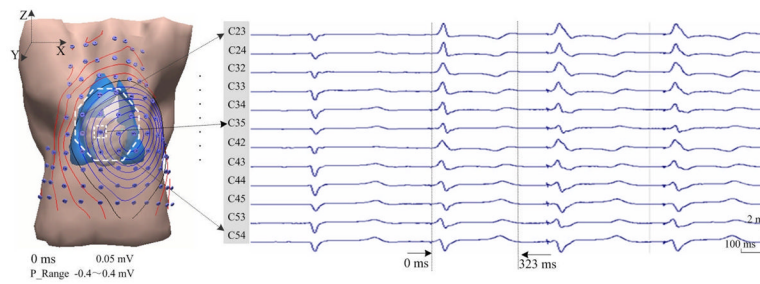
Figure 2.
Results in an animal for pacing at the site of LVL. A. Torso model with illustration of body surface electrode positions, and selected ECG waveforms within the area marked by the white dotted line on the anterior chest. B. Results during ventricular depolarization following pacing (from 17 ms after pacing spike). In subfigures B: (i) Body surface isopotential contour maps and (ii) Estimated dipole trajectory of the cardiac activation. Each isopotential map is depicted at a different time instant by the increment of 0.05 mV. In the dipole trajectory, dark blue represents the earliest activated dipole marked by 'IS' and red represents the latest activated one. The green ball represents the position of pacing stimulus marked by 'PS'. The axis of X, Y, and Z is consistent with that of torso model, which are in terms of the right-left, the posterior-anterior, and the inferior-superior, respectively.
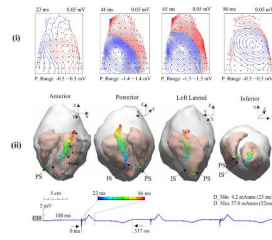
Figure 3.
Results in another animal for pacing at the site of RVA. See figure caption of Fig. 2.
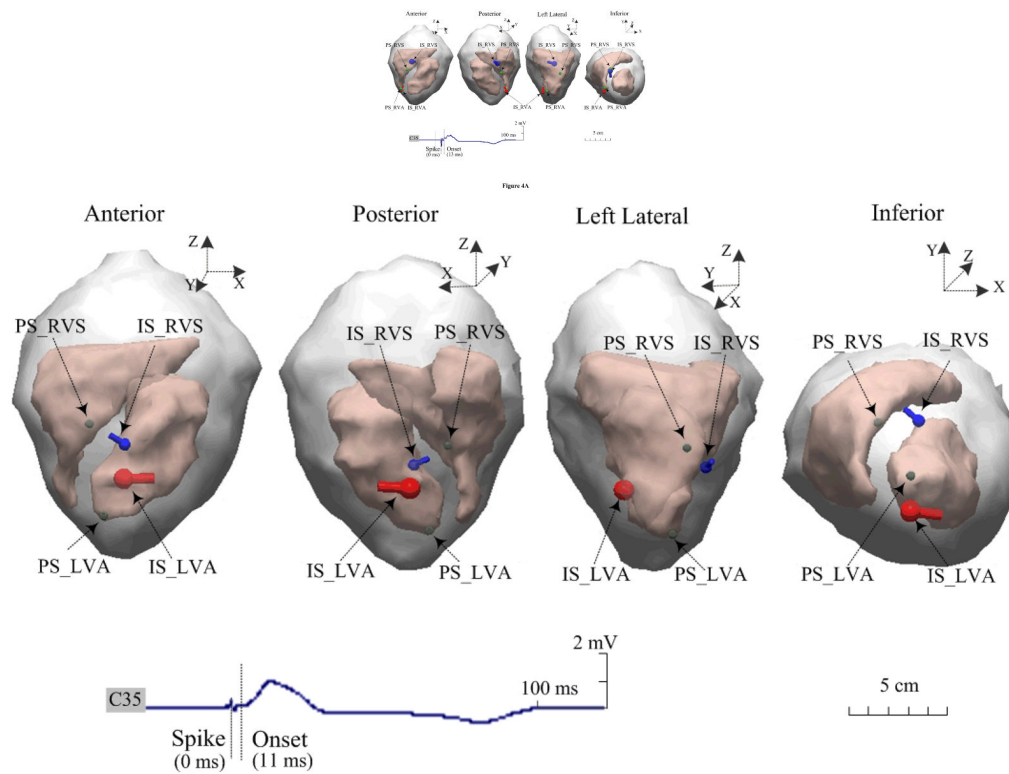
Figure 4B

Figure 4.
Estimated dipole locations during simultaneous dual-site pacing on an animal. A. The RVA-RVS sites are within a single-chamber of the RV, and B. the RVS-LVA sites are within the dual-chamber pair of the RV and LV. The blue dipole and red dipole represent the estimated dipole locations of initial sites after simultaneous pacing from the RVS and RVA or LVA sites marked by 'IS_RVS' and 'IS_RVA' or 'IS_LVA, respectively. The green ball correspondingly represents the positions of these pacing sites marked by 'PS_RVS' and 'PS_RVA' or 'PS_LVA.

TABLE 1

Experimental and Modeling Parameters

Pig No.	Heart Size (mm) $X \times Y \times Z$[†‡]	Boundary Elements (Heart surface)	Surface Electrodes	Pacing Sites	
				Single-Site Pacing	Dual-Site Pacing
1	105.3×114.5×160.5	6310 (3462)	83	RVS,LVL,LVAn	—
2	103.5×100.8×159.6	5672 (2802)	85	RVA,LVS,LVAn	—
3	113.6×108.5×140.1	5104 (2536)	88	RVA,RVS,LVL,LVS,LVAn	RVA-RVS,RVA-LVL
4	102.3×117.7×144.2	6152 (2872)	90	RVA,RVS,LVL,LVA,LVAn	RVA-RVS,RVS-LVL,RVS-LVA

[†]The axis of X, Y, and Z are consistent with the axis system of torso model referred as figure 2A, which are in terms of the right-left, the posterior-anterior, and the inferior-superior, respectively.

TABLE 2

Localization Errors for Single-Site Pacing

Pig No. and Pacing Site	Beat-to-Beat Estimation Uncertainty (mm)						Average Localization Error $D_m \pm S_d$ (mm)	Onset Instant Range (ms)
	1	2	3	4	5	6		
Endocardial LV Pacing								
1,LVL	15.8	19.0	24.3	19.9	21.2	17.1	19.6 ± 3.0	12–16
1,LVAn	21.5	20.3	25.1	23.5	29.1	26.8	24.4 ± 3.3	15–23
2,LVS	23.5	20.3	26.1	23.7	29.8	23.7	24.5 ± 3.2	10–14
2,LVAn	10.4	13.7	16.3	14.9	14.0	12.9	13.7 ± 2.0	10–15
3,LVL	16.3	14.8	17.1	7.6	16.2	20.9	15.5 ± 4.4	20–25
3,LVS	10.3	14.2	10.4	18.4	15.0	10.3	13.1 ± 3.3	23–30
3,LVAn	8.5	13.8	12.0	12.4	6.8	9.9	10.6 ± 2.6	14–22
4,LVA	19.1	31.6	35.1	23.5	22.0	35.3	27.8 ± 7.1	10–19
4,LVL	16.1	24.7	19.3	21.8	21.5	25.7	21.5 ± 3.5	11–14
4,LVAn	15.2	14.6	11.1	14.5	11.7	11.2	13.1 ± 1.9	15–18
Intramural RV Pacing								
1,RVS	18.5	22.5	21.8	11.3	22.8	15.4	18.7 ± 4.8	14–19
2,RVA	19.7	22.7	17.6	21.6	22.6	16.3	20.1 ± 2.7	15–18
3,RVA	20.0	18.7	21.9	23.1	20.8	15.5	20.0 ± 2.7	16–20
3,RVS	13.8	15.8	13.6	5.3	16.1	10.2	12.5 ± 4.1	11–16
4,RVA	13.9	15.9	19.8	17.8	14.2	13.9	15.9 ± 2.4	18–23
4,RVS	8.8	18.9	32.8	34.6	31.4	34.0	26.7 ± 10.6	11–17

TABLE 3

Localization Errors for Dual-Site Pacing

Pig No. and Pacing Site	Beat-to-Beat Estimation Uncertainty(mm)						Average Localization Error $D_m \pm S_d$ (mm)	Onset Instant Range (ms)
	1	2	3	4	5	6		
3,RVA-RVS	19.4/30.5	29.0/34.6	22.2/20.5	33.1/28.5	30.0/36.1	21.6/22.7	25.9±5.5/28.8±6.3	20–23
3,RVA-LVL	14.0/24.7	16.2/20.2	27.5/12.4	38.3/20.6	29.1/26.7	27.4/26.9	25.4±9.0/21.9±5.5	21–25
4,RVA-RVS	24.1/36.0	20.1/9.0	19.2/22.9	30.1/17.8	28.9/17.1	24.4/23.4	24.5±4.5/21.0±9.0	14–23
4,RVS-LVL	10.2/24.1	13.8/32.2	12.5/28.1	16.9/14.5	13.0/30.8	9.2/31.9	12.6±2.7/27.0±6.8	15–18
4,RVS-LVA	27.4/39.3	30.5/39.0	22.9/43.8	31.6/21.5	27.2/37.2	19.4/32.6	26.5±4.6/35.6±7.8	10–17